ELECTRONIC SEISMOLOGIST

Rapid Earthquake Association and Location

by Miao Zhang, William L. Ellsworth, and Gregory C. Beroza

ABSTRACT

Rapid association of seismic phases and event location are crucial for real-time seismic monitoring. We propose a new method, named rapid earthquake association and location (REAL), for associating seismic phases and locating seismic events rapidly, simultaneously, and automatically. REAL combines the advantages of both pick-based and waveform-based detection and location methods. It associates arrivals of different seismic phases and locates seismic events primarily through counting the number of *P* and *S* picks and secondarily from travel-time residuals. A group of picks are associated with a particular earthquake if there are enough picks within the theoretical travel-time windows. The location is determined to be at the grid point with the most picks, and if multiple locations have the same maximum number of picks, the grid point among them with smallest travel-time residuals. We refine seismic locations using a least-squares location method (VELEST) and a high-precision relative location method (hypoDD). REAL can be used for rapid seismic characterization due to its computational efficiency. As an example application, we apply REAL to earthquakes in the 2016 central Apennines, Italy, earthquake sequence occurring during a five-day period in October 2016, midway in time between the two largest earthquakes. We associate and locate more than three times as many events (3341) as are in Italy's National Institute of Geophysics and Volcanology routine catalog (862). The spatial distribution of these relocated earthquakes shows a similar but more concentrated pattern relative to the cataloged events. Our study demonstrates that it is possible to characterize seismicity automatically and quickly using REAL and seismic picks.

Supplemental Content: Figures detailing further location sensitivity analysis.

INTRODUCTION

Earthquake detection and location methods are generally divided into two main classes: pick-based methods and waveform-based methods (Pesicek *et al.*, 2014; Grigoli *et al.*, 2018; and references therein). Standard pick-based detection and location methods consist of three main sequential steps: (1) phase detection and picking, (2) phase association, and (3) event location (Grigoli *et al.*, 2018). The first step includes seismic phase detection and arrival-time picking, which are performed based on the change of amplitude, energy, frequency, or polarization of waveforms (Allen, 1978, 1982; Baer and Kradolfer, 1987; Magotra *et al.*, 1987; Cichowicz, 1993; Withers *et al.*, 1998; Bai and Kennett, 2000; Lomax *et al.*, 2012; Baillard *et al.*, 2013) or determined by similarity, such as using artificial intelligence algorithms (e.g., Mousavi *et al.*, 2018; Perol *et al.*, 2018; Ross *et al.*, 2018; Zhu and Beroza, 2019; Zhu *et al.*, 2019).

Phase association groups those picks that best fit the different phase types associated with a particular earthquake (Allen, 1982; Johnson *et al.*, 1997; Grigoli *et al.*, 2018) using simple grouping strategies (e.g., Stewart, 1977), sophisticated clustering algorithms (Ester *et al.*, 1996; Zhu *et al.*, 2017), constant relative event time (Bergen and Beroza, 2018), artificial intelligence algorithms (McBrearty *et al.*, 2019; Ross *et al.*, 2019), or other advanced algorithms based on the principle of travel-time back projection (Dietz, 2012; Johnson *et al.*, 1997; Patton *et al.*, 2016) and Bayesian probability theory (Arora *et al.*, 2013). Phase types (e.g., *P* or *S*) are interpreted during detection or automatically identified during association. Event location is determined by minimizing the travel-time residuals between theoretical and observed (picked) seismic phases (usually *P* and *S* phases) using linearized (e.g., Thurber, 1985) or global (e.g., Lomax *et al.*, 2000) inversion algorithms.

Waveform-based methods, independent of seismic phase picking, detect, associate, and locate earthquakes simultaneously in a single step by maximizing the stacked waveform energy or coherence using the delay-and-sum concept (e.g., Kao and Shan, 2004; Grigoli *et al.*, 2013; Zhang and Wen, 2015), which are sensitive to weak signals and enable us to detect small earthquakes. They are computationally expensive, however, due to the need for an exhaustive search of potential locations in 3D space and potential origin times, sample by sample, in continuous data. Pick-based methods are widely used in routine seismic monitoring due to their high-computational efficiency; however, waveform-based methods generally perform better than pick-based methods in detecting small events (e.g., Kao and Shan, 2004; Grigoli *et al.*, 2013, 2018; Pesicek *et al.*, 2014; Yoon *et al.*, 2015, 2017; Zhang and

 doi: 10.1785/0220190052

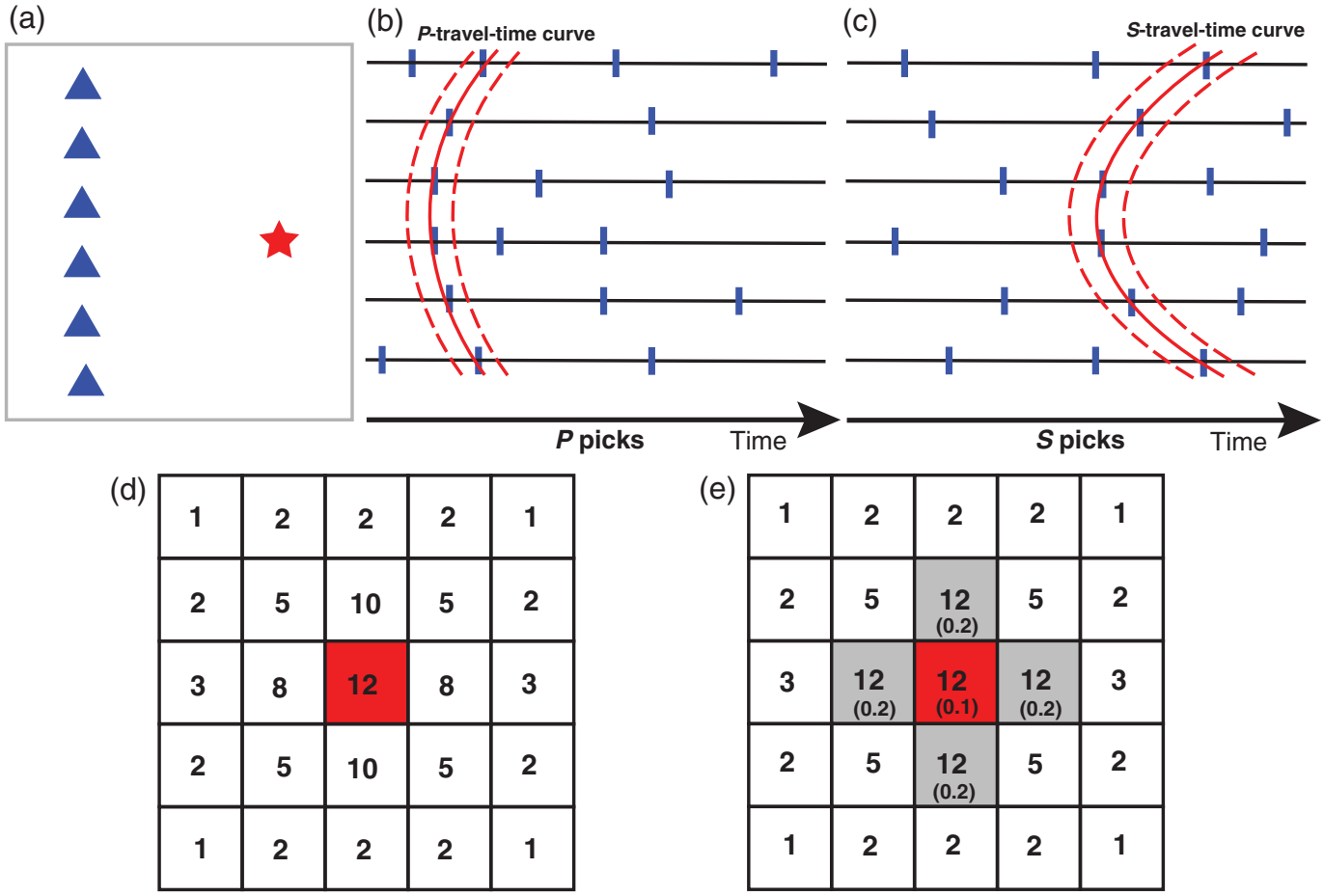

1	2	2	2	1
2	5	10	5	2
3	8	12	8	3
2	5	10	5	2
1	2	2	2	1

1	2	2	2	1
2	5	12 (0.2)	5	2
3	12 (0.2)	12 (0.1)	12 (0.2)	3
2	5	12 (0.2)	5	2
1	2	2	2	1

▲ **Figure 1.** Cartoon illustrating the concept of rapid earthquake association and location (REAL) for earthquake association and location. (a) The distribution of seismic event (red star) and seismic stations (blue triangles). (b) *P* arrival-time curve (red curve) with its uncertainty range (red dashed curves) due to velocity uncertainty and limited searching interval, associated *P* picks and other false *P* picks. (c) Same as (b) but for *S* phase. (d) The optimal location is determined to be at the grid point with most picks or (e) the grid point with smallest travel-time residual (shown in bottom parentheses, and its unit is second) and most picks if multiple locations have the same maximum number of picks.

Wen, 2015; Tong *et al.*, 2016; Li *et al.*, 2017; Perol *et al.*, 2018).

In this study, we propose an automatic and simultaneous earthquake association and location method: rapid earthquake association and location (REAL). Using the delay-and-sum concept, we associate and locate earthquakes using *P* and *S* picks obtained with a conventional short-term average/long-term average (STA/LTA) picker. We introduce the association and location procedure, illustrate its effectiveness using synthetic tests, demonstrate REAL on five days of continuous seismic records in central Apennines, Italy, and compare our results with Italy's National Institute of Geophysics and Volcanology (INGV) catalog.

METHOD

Waveform-based earthquake detection and location methods based on the delay-and-sum concept have been developed and widely used in seismological studies for both absolute seismic locations (e.g., Kao and Shan, 2004; Grigoli *et al.*, 2013) and relative seismic locations (e.g., Zhang and Wen, 2015). Compared to traditional pick-based earthquake detection and location methods, these methods are independent of seismic phase detection, picking, identification, and association using continuous seismic records instead of phase picks. However, they generally have not been applied to rapid seismic characterization due to their exhaustive searching in space and time. Consequently, pick-based methods are still the preferred solution for real-time seismological applications (Grigoli *et al.*, 2018). Here, we apply the delay-and-sum strategy to seismic picks rather than continuous seismic data. REAL associates seismic *P* and *S* picks (arrivals) to a particular event and locates it simultaneously through counting the number of seismic picks and calculating travel-time residuals rather than scanning the entire waveform (or its characteristic function) and estimating the brightness (energy) or the coherence sample by sample (Fig. 1). This dramatically reduces the computation time because we use very limited phase picks that are far fewer

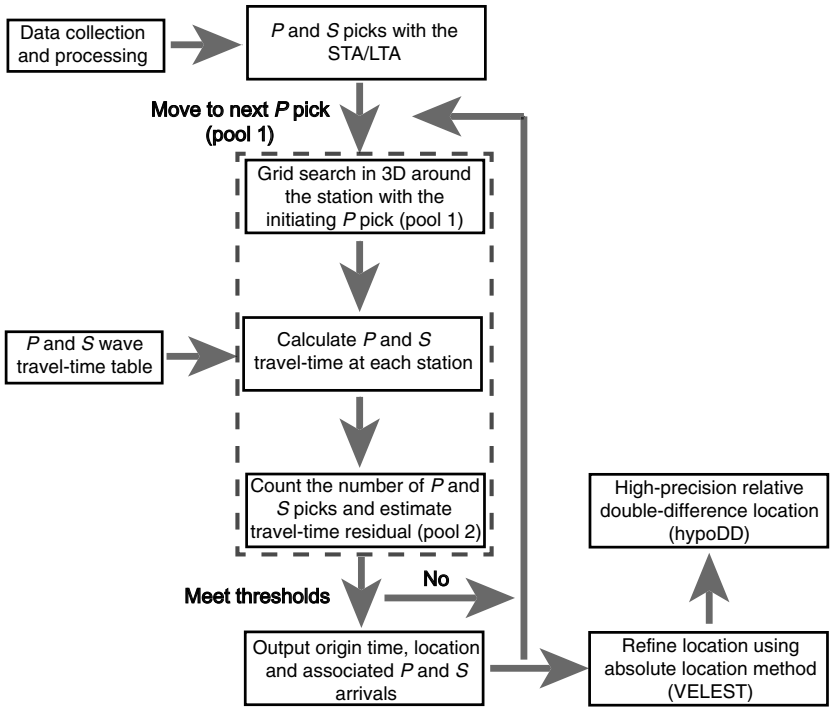

▲ **Figure 2.** Flow diagram of REAL. The dashed rectangle indicates the parallel programming part.

than the number of continuous data samples (or time windows). Figure 2 shows a flow diagram that describes how the REAL algorithm works.

REAL consists of three main steps as follows:

- *Step 1: Phase triggering and amplitude estimation*. We calculate the horizontal (including east and west components) and vertical energy (vertical component) of the waveforms recorded at each three-component station and apply a recursive STA/LTA algorithm to these energy traces (Grigoli *et al.*, 2013). *P* and *S* picks, along with their STA/LTA ratios, are determined from the vertical and horizontal traces, respectively. Only the pick with the highest STA/LTA ratio will be kept in REAL if multiple picks appear within a specified time window (e.g., 5 s). To calculate earthquake magnitude in the following step, we also estimate horizontal-component amplitudes for picked *P* and *S* phases after deconvolving raw waveforms with the instrument response and then convolving the obtained signal with the theoretical Wood–Anderson seismometer response (Hutton and Boore, 1987). Therefore, our inputs include first arrivals of the *P* and *S* phases, their STA/LTA ratios and amplitudes. Phase amplitudes are optional and are used in magnitude estimation as needed.
- *Step 2: Grid search and objective function calculation*. We use *P* picks to initiate the procedure because they are typically more reliable than *S* picks. We search potential locations in 3D around the station with the earliest *P* arrival (i.e., the initiating pick). The horizontal search range is dependent on the average station interval, and the depth range is from the surface to a specified depth (e.g., 30 km for crustal earthquakes). We precalculate theoretical *P* and *S* travel-time tables using the TauP Toolkit (Crotwell *et al.*, 1999) and given velocity model. Without loss of generality, we utilize 1D velocity models, but we could easily extend REAL to 3D velocity models. A time window around the theoretical arrivals is adaptively determined to tolerate the model inaccuracy and the grid spacing. We first count the number of the observed *P* and *S* picks that locate within the theoretical travel-time windows and then calculate travel-time residuals if multiple grid points have the same maximum number of picks. We perform grid search in parallel using a shared memory programming paradigm (OpenMP).
- *Step 3: Criteria and feedback*. We propose two criteria to associate and locate an event in REAL: (1) at least one grid meets the criterion: the number of observed *P* and *S* picks that appear in the predicted time windows exceeds a preset threshold, and (2) the optimal event location is determined to be at the grid point with the maximum number of associated *P* and *S* picks, or if multiple grid points have the same maximum number of picks, the grid point with the most picks and the smallest travel-time residual. Similar to waveform-based earthquake detection and location methods (e.g., Kao and Shan, 2004; Shelly *et al.*, 2007; Peng and Zhao, 2009), we keep the most reliable event within a specified time window (e.g., 5 s). Threshold settings would empirically change with the number of stations, as well as pick quality (e.g., uncertainty and reliability). Once an earthquake is associated and located, we calculate its local magnitude using the corrected amplitudes of the associated phases and a widely used empirical amplitude-and-local-magnitude relationship (Hutton and Boore, 1987).

We have two pools of picks in our algorithm. Pool one only includes *P* picks as initiating picks. An initiating *P* pick will be removed from pool one after the current association process whether or not it associates with an event. If an event was declared, associated *P* picks are also removed from pool one. The oldest remaining *P* pick in pool one initiates a new association process. Pool two is used to count the number of *P* and *S* picks, calculate the travel-time residuals, and estimate earthquake magnitude. It contains all available *P* and *S* picks and their Wood–Anderson amplitudes. It does not change, which enables us to calculate the number of picks and travel-time residuals for each potential event with the same pick dataset.

The location accuracy and efficiency trade-off depends on the number of seismic picks, the size of grid search, and the accuracy of velocity model. To minimize potentially unstable

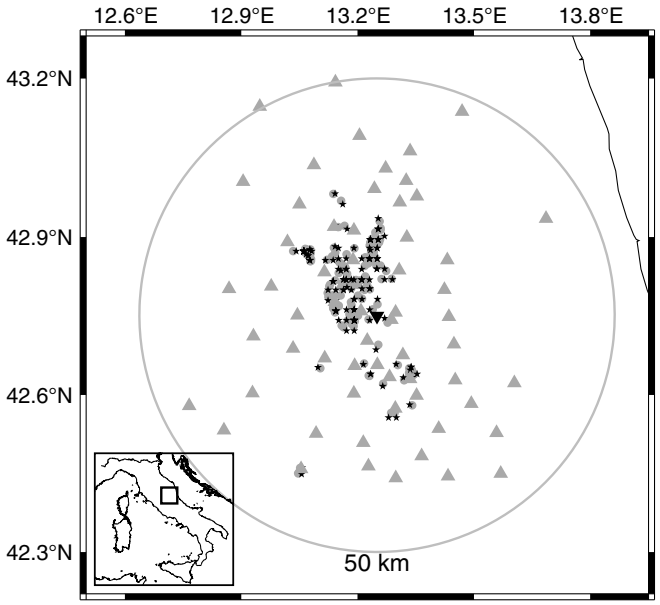

▲ **Figure 3.** Map showing seismic stations (triangles) within 50 km of the earthquake sequence, 151 Institute of Geophysics and Volcanology (INGV) cataloged events (gray dots), and their locations determined by REAL (black stars) in synthetic test. Inverted triangle represents the event used for location resolution test in Figure 4. (Inset) Regional map of Italy, with the rectangle indicating the study region.

detections around the boundary of the study area, we remove events with large station gaps (e.g., >200°). We provide interfaces to refine earthquake locations using a least-squares location software VELEST (Kissling *et al.*, 1994) and a high-precision relative location software hypoDD (Waldhauser and Ellsworth, 2000). Therefore, we bridge the gap between the raw continuous seismic data and high-precision earthquake locations using a conventional STA/LTA picker, REAL, and open-source location software.

SYNTHETIC VALIDATION

We use synthetic data to test the performance of REAL and evaluate its reliability and robustness. We apply REAL to associate and locate earthquakes in the central Apennines, Italy, on 14 October 2016, the first day of the field data in the next section. Sixty high-quality broadband seismic stations are located within 50 km of the sequence (Fig. 3), including both permanent stations and those deployed after the first mainshock of the 2016 earthquake sequence (Michele *et al.*, 2016; Moretti *et al.*, 2016). INGV published 151 earthquakes with a magnitude range of 0.6–3.3 in the study area. In this section, we use these 151 cataloged events as our synthetic events. A 1D layer velocity model is employed in the target area (Chiaraluce *et al.*, 2017).

To simulate *P* and *S* picks, we first calculate *P* and *S* travel time for each event at 60 seismic stations using the TauP Toolkit (Crotwell *et al.*, 1999). *P* and *S* travel-time tables are calculated and stored in distance and depth. The searched area for the potential event location is 0.2° in latitude and 0.2° in longitude with a searching interval of 0.02° (appropriate 1.5 km) and 30 km in depth with a search interval of 2 km, centered at the station that recorded the initiating *P* phase. The threshold is consistent with the field application in the next section. All 151 events, including their locations, are recovered after applying REAL. The mean location uncertainty is determined to be 0.74 km in horizontal direction and 0.57 km in depth, which is less than the grid interval. To test the effect of inaccurate velocity structure, we employ REAL to associate and locate these events using an averaged homogenous *P* and *S* velocities (i.e., 6.2 and 3.3 km/s) instead of the known 1D layer velocity model. All events are recovered with a mean location uncertainty of 0.76 km in the horizontal and 0.57 km in depth. We randomly add perturbations to the observed *P* and *S* arrivals to simulate the inaccurate time picking. All events are recovered with an acceptable location uncertainty when we randomly vary the *P* and *S* arrivals from 0 to 0.2 s and from 0 to 0.4 s, respectively.

With a fine search grid (0.001° in latitude and longitude and 0.1 km in depth), we analyze event location convergence using a synthetic event near the center of the network (i.e., [42.75°, 13.25°, 10 km]). This event is fully recovered along with its location after applying REAL. Figure 4 shows the distribution of the number of associated *P* and *S* picks (120 picks in total), as well as the distribution of travel-time residuals over the grids that have the same maximum number of picks. The total number of picks converges toward the target point (Fig. 4a), and the optimal location is further determined from travel-time residual (Fig. 4b). To simulate a less well-observed event, we randomly select 18 *P* and *S* picks from the total 120 picks. REAL successfully associates the 18 picks with this event and recovers its location as well (Ⓔ Fig. S1, available in the supplemental content to this article). To test the tolerance of REAL to false triggers, we randomly add false picks for both *P* and *S* phases at the 60 stations, ranging from the earliest *P* pick to the latest *S* pick. On average, one false pick would appear every 4.25 s. This event is recovered with a well-constrained location when the number of false picks is up to four times greater than the real ones (Ⓔ Fig. S2), which indicates that REAL is robust with respect to false picks.

APPLICATION TO FIVE DAYS CONTINUOUS DATA IN 2016 CENTRAL APENNINES, ITALY, EARTHQUAKE SEQUENCE

In this section, we apply REAL to seismic data recorded over five days (from 14 October 2018 to 18 October 2018) midway in time between the two largest earthquakes in the 2016 central Apennines, Italy, earthquake sequence. We first detect and pick *P* and *S* phases from vertical and horizontal components, respectively, using continuous three-component seismic data and a recursive STA/LTA algorithm (Grigoli *et al.*, 2013), then estimate horizontal-component amplitudes for triggered *P* and *S* phases after convolving them with a standard Wood–Anderson

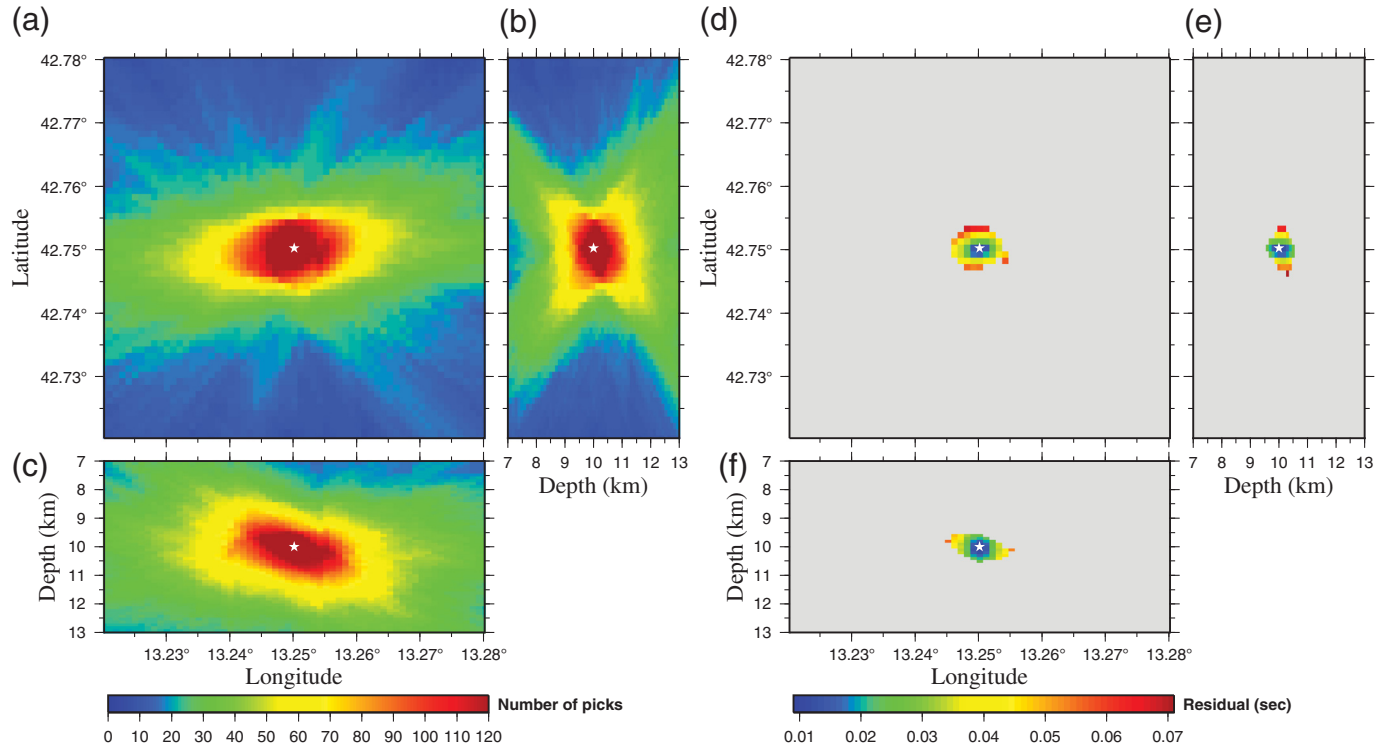

▲ **Figure 4.** (a) Distribution of number of *P* and *S* picks in longitude–latitude plane, (b) latitude-depth plane and (c) longitude-depth plane when applying REAL to associate and locate the synthetic event shown in Figure 3. (d–f) Distribution of travel-time residuals over the grids in (a–c) with the same maximum number of picks (120). White stars represent the optimal location determined by REAL.

seismometer instrument response (Hutton and Boore, 1987). We use the same search area and search interval as used in the synthetic test. We empirically set the threshold to five *P* picks and a total of 18 *P* and *S* picks (i.e., 15% of the total potential 120 picks) and remove events occurring close to the boundary of the study area or with a station gap of larger than 200°. We associate 3341 events in the five-day interval. REAL recovers all $\mathbf{M} \geq 1.0$ events (835) in the INGV monitoring room catalog. Twenty-seven small events ($\mathbf{M} < 1.0$) escape the detection and location for three possible reasons (1) deficient seismic phase picking, (2) their locations are close to the boundaries of our study area, or (3) they occurred closely after other large events. We estimate the approximate magnitudes of completeness for the REAL and INGV catalogs using the same amplitude-and-local-magnitude relationship (Hutton and Boore, 1987). The REAL catalog has a completeness of magnitude 0.4 compared to 1.0 for the INGV catalog (Fig. 5). The size of the search grid cells limits our location accuracy (Figs. 6b and 7a). To improve the location accuracy, we repick the associated arrivals using an Akaike information criterion picker (Maeda, 1985) and relocate the earthquakes. We refine the locations using a least-squares location method, VELEST (Kissling *et al.*, 1994), based on those associated arrivals and initial locations (Figs. 6c and 7b). The median travel-time residual reduces from 0.25 to 0.2 s. We then employ the double-difference location method hypoDD (Waldhauser and Ellsworth, 2000) to improve the relative locations of 3023 events (Figs. 6d and 7c). The median travel-time residual further reduces to 0.06 s. The distribution of our associated and relocated events shows a similar but more concentrated pattern than the INGV catalog (Figs. 6 and 7).

DISCUSSION

REAL is based on the idea of delay-and-sum, but it differs from previous methods that use the delay-and-sum concept. We

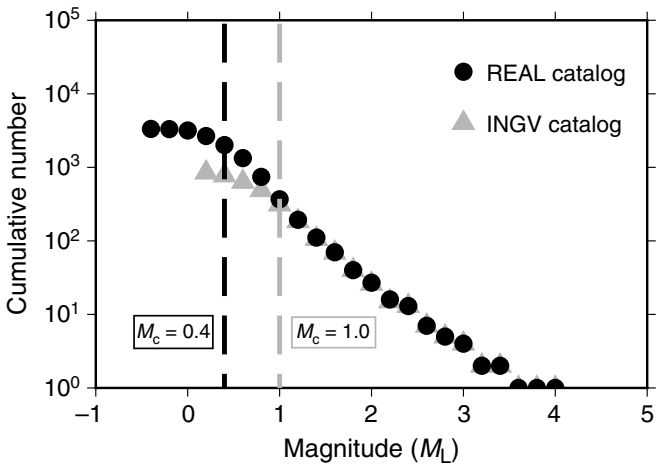

▲ **Figure 5.** Frequency–magnitude distribution and magnitude of completeness (M_c) for the REAL and INGV monitoring room catalogs.

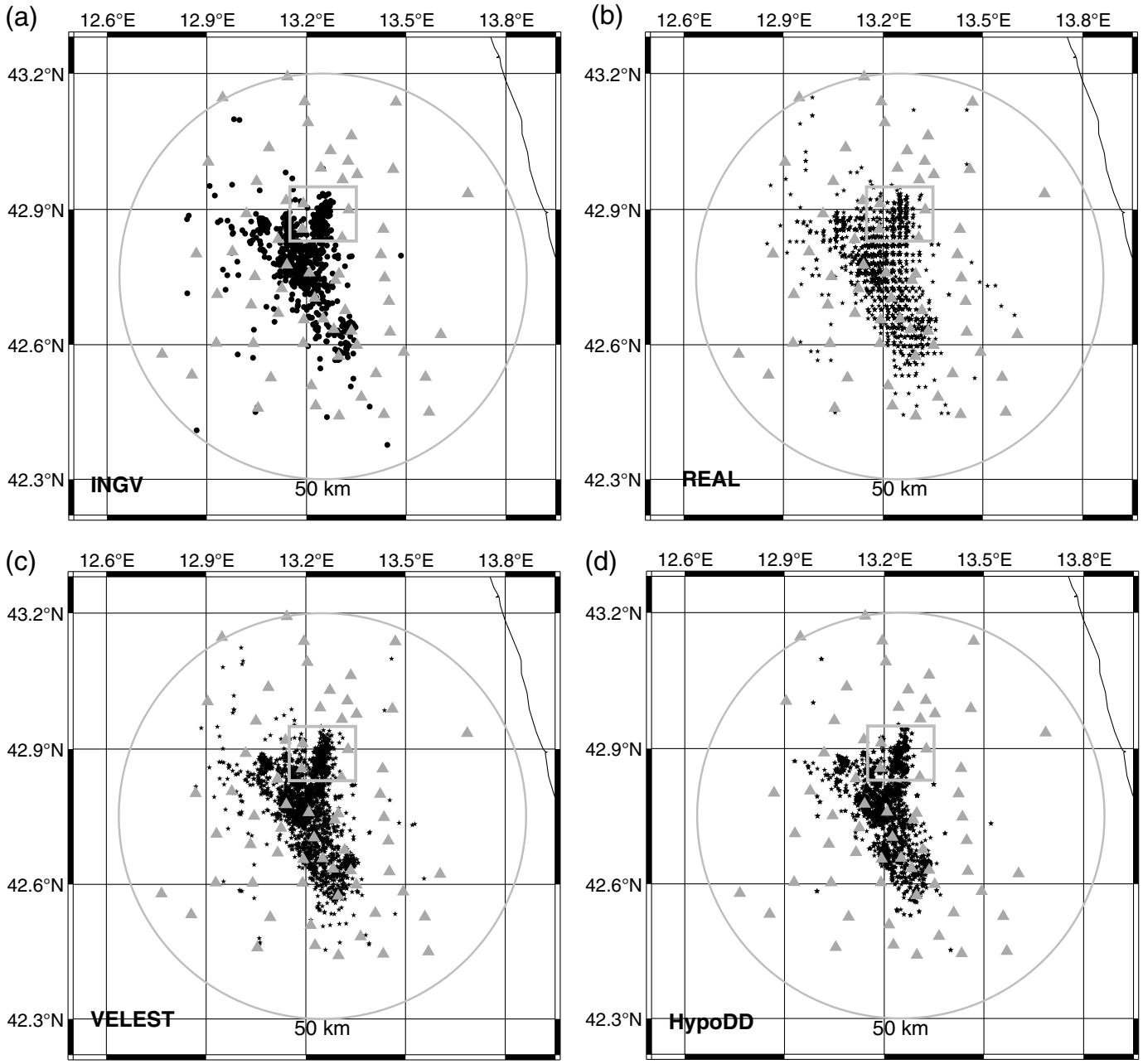

▲ **Figure 6.** Earthquake location comparison between (a) INGV cataloged events (dots), (b) blindly associated events (stars) identified by REAL, (c) locations refined by VELEST, and (d) relocations using hypoDD. Triangles represent seismic stations used in this study. Gray rectangle marks zoomed-in area in Figure 7.

count the associated seismic picks as our objective function rather than enhance the energy or coherence of the seismic waveform (or its characteristic). The spatial travel-time residual is used as supplemental information to determine the optimal location. Compared to the source-scanning algorithm (Kao and Shan, 2004), REAL uses limited seismic picks rather than continuous data. This reduces the computational cost. The computational efficiency depends on the number of seismic picks, search area, and grid spacing. To accelerate the association and location process, we only utilize those *P* and *S* picks in a limited time window following the initiating *P* pick. The time range depends on the travel time across the study area. For one day of data in this study, it takes only seconds for hundreds of picks and minutes for thousands of picks on a MacBook laptop computer (3.1 GHz quad-core Intel Core i7 processor).

As suggested in our synthetic tests, REAL can determine earthquake location accurately if we have a sufficient number of phase picks, a fine-enough searching interval, and a reasonably accurate velocity model. Other seismic detection and

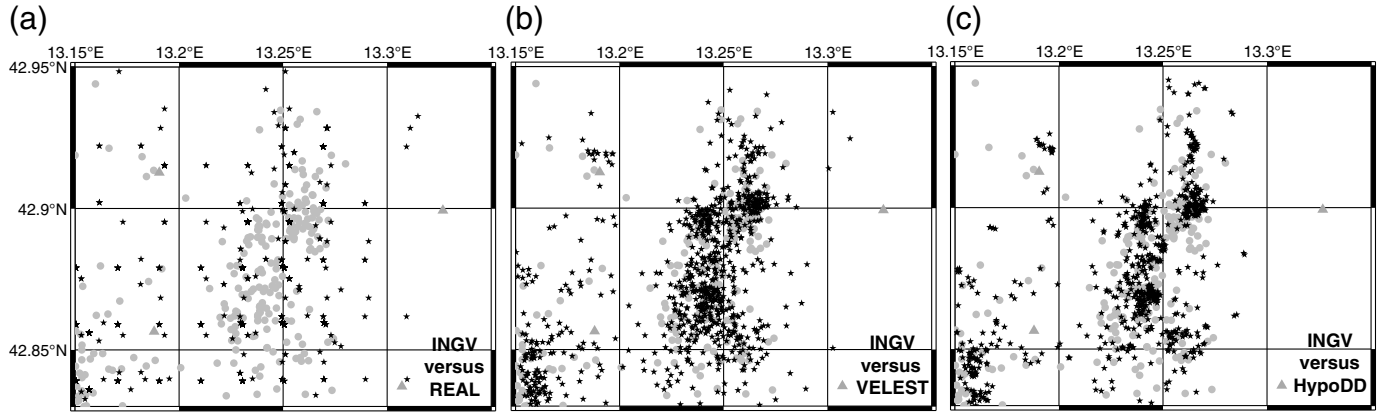

▲ **Figure 7.** Comparison of earthquake locations for the INGV (gray dots) and REAL catalogs (black stars). INGV locations are common to all panels. REAL locations from (a) initial grid detections, (b) locations after repicking and location with VELEST, and (c) relocation using hypoDD.

picking methods can be used in phase picking step (e.g., Lomax *et al.*, 2012; Chen and Holland, 2016; Zhu and Beroza, 2019; Zhu *et al.*, 2019) to improve location precision. Additional phases (e.g., *pP*, *sP*) can also be used to improve location accuracy, as long as the corresponding travel-time tables are provided. Although we only tested REAL for regional earthquake association, it should be straightforward to extend it to global monitoring using a global travel-time table. In addition to the dense station coverage case, REAL can successfully deal with the sparse station coverage case as well (Wang *et al.*, 2018). It is also possible to apply REAL to real-time seismic monitoring using *P* picks alone.

REAL possesses the main advantages of both pick-based and waveform-based detection and location methods. Waveform-based methods search for events in 3D space in the whole study region using continuous seismic data. REAL searches for a smaller area around the station with the current initiating phase and seismic picks rather than continuous data. This reduces the computational cost. A potential limitation of REAL is that it may not detect weak events as well as the waveform-based methods, due to the limitations of phase picking methods. REAL differs from the standard pick-based methods in three aspects: (1) REAL associates and locates seismic events simultaneously rather than separately using seismic picks; (2) REAL automatically excludes those unlikely seismic picks (outliers) that can lead to missing earthquakes or false detections and large location uncertainties; and (3) the objective function in REAL includes both the number of seismic picks (similar to the stacking process in waveform-based methods) and the travel-time residual (as in standard pick-based methods). In other words, REAL combines the computational efficiency of standard pick-based methods and the location accuracy of waveform-based methods. On the other hand, REAL also inherits some of the disadvantages from waveform-based methods, such as that it only keeps the most reliable event within a time window and can miss events that occur closely in space and time.

CONCLUSIONS

Rapid earthquake detection and characterization is a crucial task in earthquake seismology. Pick-based detection and location methods still dominate in routine seismic monitoring due to their high-computational efficiency. We present a novel method, REAL, for rapidly and simultaneously associating and locating earthquakes using the concept of delay-and-sum for *P* and *S* picks. This method combines the computational efficiency and location accuracy from pick-based and waveform-based methods, respectively. We associate and locate 3341 seismic events during five days in central Apennines, Italy, which is more than three times as many as are in the INGV routine catalog. We demonstrate that it is practical to detect and locate earthquakes, automatically, rapidly, and precisely using conventional phase pickers, REAL, and available high-precision earthquake-location methods.

DATA AND RESOURCES

Seismic data were downloaded from Italy's National Institute of Geophysics and Volcanology (INGV) and Incorporated Research Institutions for Seismology (IRIS) though the International Federation of Digital Seismograph Networks (FDSN) web services (http://www.fdsn.org/, last accessed February 2019). The earthquake catalog used in this study can be downloaded from http://cnt.rm.ingv.it/ (last accessed February 2019). Some figures in this article were generated using the Generic Mapping Tool (Wessel *et al.*, 2013). The rapid earthquake association and location (REAL) software can be downloaded from https://github.com/Dal-mzhang/REAL (last accessed June 2019).

ACKNOWLEDGMENTS

This work was supported by National Science Foundation (NSF) Grant Number EAR-1759810 and the Stanford Center for Induced and Triggered Seismicity (SCITS). The

authors thank Francesco Grigoli and Seyed Mostafa Mousavi for reviews in preparation of the article. The authors also thank Honn Kao, Editor-in-Chief Zhigang Peng, and an anonymous reviewer for their comments, which greatly improved the article.

REFERENCES

Allen, R. (1982). Automatic phase pickers: Their present use and future prospects, *Bull. Seismol. Soc. Am.* **72,** S225–S242.

Allen, R. V. (1978). Automatic earthquake recognition and timing from single traces, *Bull. Seismol. Soc. Am.* **68,** 1521–1532.

Arora, N. S., S. Russell, and E. Sudderth (2013). NET-VISA: Network processing vertically integrated seismic analysis, *Bull. Seismol. Soc. Am.* **103,** 709–729.

Baer, M., and U. Kradolfer (1987). An automatic phase picker for local and teleseismic events, *Bull. Seismol. Soc. Am.* **77,** 1437–1445.

Bai, C.-Y., and B. Kennett (2000). Automatic phase-detection and identification by full use of a single three-component broadband seismogram, *Bull. Seismol. Soc. Am.* **90,** 187–198.

Baillard, C., W. C. Crawford, V. Ballu, C. Hibert, and A. Mangeney (2013). An automatic kurtosis-based P- and S-phase picker designed for local seismic networks, *Bull. Seismol. Soc. Am.* **104,** 394–409.

Bergen, K. J., and G. C. Beroza (2018). Detecting earthquakes over a seismic network using single-station similarity measures, *Geophys. J. Int.* **213,** 1984–1998.

Chen, C., and A. A. Holland (2016). PhasePApy: A robust pure Python package for automatic identification of seismic phases, *Seismol. Res. Lett.* **87,** 1384–1396.

Chiaraluce, L., R. Di Stefano, E. Tinti, L. Scognamiglio, M. Michele, E. Casarotti, M. Cattaneo, P. De Gori, C. Chiarabba, and G. Monachesi (2017). The 2016 central Italy seismic sequence: A first look at the mainshocks, aftershocks, and source models, *Seismol. Res. Lett.* **88,** 757–771.

Cichowicz, A. (1993). An automatic S-phase picker, *Bull. Seismol. Soc. Am.* **83,** 180–189.

Crotwell, H. P., T. J. Owens, and J. Ritsema (1999). The TauP Toolkit: Flexible seismic travel-time and ray-path utilities, *Seismol. Res. Lett.* **70,** 154–160.

Dietz, L. (2012). Notes on configuring binder_ew: Earthworm's phase associator, available at http://love.isti.com/trac/ew/wiki/binder_ew (last accessed February 2019).

Ester, M., H.-P. Kriegel, J. Sander, and X. Xu (1996). A density-based algorithm for discovering clusters in large spatial databases with noise, *KDD-96*, 226–231.

Grigoli, F., S. Cesca, O. Amoroso, A. Emolo, A. Zollo, and T. Dahm (2013). Automated seismic event location by waveform coherence analysis, *Geophys. J. Int.* **196,** 1742–1753.

Grigoli, F., L. Scarabello, M. Böse, B. Weber, S. Wiemer, and J. F. Clinton (2018). Pick-and waveform-based techniques for real-time detection of induced seismicity, *Geophys. J. Int.* **213,** 868–884.

Hutton, L., and D. M. Boore (1987). The ML scale in southern California, *Bull. Seismol. Soc. Am.* **77,** 2074–2094.

Johnson, C. E., A. G. Lindh, and B. F. Hirshorn (1997). Robust regional phase association, *U.S. Geol. Surv. Open-File Rept. 94-621*, doi: 10.3133/ofr94621.

Kao, H., and S.-J. Shan (2004). The source-scanning algorithm: Mapping the distribution of seismic sources in time and space, *Geophys. J. Int.* **157,** 589–594.

Kissling, E., W. Ellsworth, D. Eberhart-Phillips, and U. Kradolfer (1994). Initial reference models in local earthquake tomography, *J. Geophys. Res.* **99,** 19,635–19,646.

Li, L., D. Becker, H. Chen, X. Wang, and D. Gajewski (2017). A systematic analysis of correlation-based seismic location methods, *Geophys. J. Int.* **212,** 659–678.

Lomax, A., C. Satriano, and M. Vassallo (2012). Automatic picker developments and optimization: FilterPicker—A robust, broadband picker for real-time seismic monitoring and earthquake early warning, *Seismol. Res. Lett.* **83,** 531–540.

Lomax, A., J. Virieux, P. Volant, and C. Berge-Thierry (2000). Probabilistic earthquake location in 3D and layered models, in *Advances in Seismic Event Location*, C. H. Thurber and N. Rabinowitz (Editors), Kluwer, Amsterdam, The Netherlands, 101–134.

Maeda, N. (1985). A method for reading and checking phase times in autoprocessing system of seismic wave data, *Zisin* **38,** 365–379.

Magotra, N., N. Ahmed, and E. Chael (1987). Seismic event detection and source location using single-station (three-component) data, *Bull. Seismol. Soc. Am.* **77,** 958–971.

McBrearty, I. W., A. A. Delorey, and P. A. Johnson (2019). Pairwise association of seismic arrivals with convolutional neural networks, *Seismol. Res. Lett.* **90,** 503–509.

Michele, M., R. Di Stefano, L. Chiaraluce, M. Cattaneo, P. De Gori, G. Monachesi, D. Latorre, S. Marzorati, L. Valoroso, and C. Ladina (2016). The Amatrice 2016 seismic sequence: A preliminary look at the mainshock and aftershocks distribution, *Ann. Geophys.* **59,** doi: 10.4401/ag-7227.

Moretti, M., S. Pondrelli, L. Margheriti, L. Abruzzese, M. Anselmi, P. Arroucau, P. Baccheschi, B. Baptie, R. Bonadio, and A. Bono (2016). SISMIKO: Emergency network deployment and data sharing for the 2016 central Italy seismic sequence, *Ann. Geophys.* **59,** doi: 10.4401/ag-7212.

Mousavi, S. M., W. Zhu, Y. Sheng, and G. C. Beroza (2018). CRED: A deep residual network of convolutional and recurrent units for earthquake signal detection, available at http://arxiv.org/abs/1810.01965 (last accessed February 2019).

Patton, J. M., M. R. Guy, H. M. Benz, R. P. Buland, B. K. Erickson, and D. S. Kragness (2016). Hydra—The National Earthquake Information Center's 24/7 seismic monitoring, analysis, catalog production, quality analysis, and special studies tool suite, *U.S. Geol. Surv. Open-File Rept. 2016-1128*, doi: 10.3133/ofr20161128.

Peng, Z., and P. Zhao (2009). Migration of early aftershocks following the 2004 Parkfield earthquake, *Nat. Geosci.* **2,** 877.

Perol, T., M. Gharbi, and M. Denolle (2018). Convolutional neural network for earthquake detection and location, *Sci. Adv.* **4,** e1700578, doi: 10.1126/sciadv.1700578.

Pesicek, J. D., D. Child, B. Artman, and K. Cieślik (2014). Picking versus stacking in a modern microearthquake location: Comparison of results from a surface passive seismic monitoring array in Oklahoma, *Geophysics* **79,** KS61–KS68.

Ross, Z. E., M. A. Meier, and E. Hauksson (2018). P-wave arrival picking and first-motion polarity determination with deep learning, *J. Geophys. Res.* **123,** 5120–5129.

Ross, Z. E., Y. Yue, M. A. Meier, E. Hauksson, and T. H. Heaton (2019). PhaseLink: A deep learning approach to seismic phase association, *J. Geophys. Res.* **124,** 856–869.

Shelly, D. R., G. C. Beroza, and S. Ide (2007). Non-volcanic tremor and low-frequency earthquake swarms, *Nature* **446,** 305.

Stewart, S. W. (1977). Real-time detection and location of local seismic events in central California, *Bull. Seismol. Soc. Am.* **67,** 433–452.

Thurber, C. H. (1985). Nonlinear earthquake location: theory and examples, *Bull. Seismol. Soc. Am.* **75,** 779–790.

Tong, P., D. Yang, Q. Liu, X. Yang, and J. Harris (2016). Acoustic wave-equation-based earthquake location, *Geophys. J. Int.* **205,** 464–478.

Waldhauser, F., and W. L. Ellsworth (2000). A double-difference earthquake location algorithm: Method and application to the northern Hayward fault, California, *Bull. Seismol. Soc. Am.* **90,** 1353–1368.

Wang, K., W. L. Ellsworth, G. C. Beroza, G. Williams, M. Zhang, D. Schroeder, and J. Rubinstein (2018). Seismology with dark data: Image-based processing of analog records using machine learning

for the Rangely earthquake control experiment, *Seismol. Res. Lett.* **90,** no. 2A, 553–562, doi: 10.1785/0220180298.

Wessel, P., W. H. Smith, R. Scharroo, J. Luis, and F. Wobbe (2013). Generic mapping tools: Improved version released, *Eos Trans. AGU* **94,** 409–410.

Withers, M., R. Aster, C. Young, J. Beiriger, M. Harris, S. Moore, and J. Trujillo (1998). A comparison of select trigger algorithms for automated global seismic phase and event detection, *Bull. Seismol. Soc. Am.* **88,** 95–106.

Yoon, C. E., Y. Huang, W. L. Ellsworth, and G. C. Beroza (2017). Seismicity during the initial stages of the Guy-Greenbrier, Arkansas, earthquake sequence, *J. Geophys. Res.* **122,** 9253–9274.

Yoon, C. E., O. O'Reilly, K. J. Bergen, and G. C. Beroza (2015). Earthquake detection through computationally efficient similarity search, *Sci. Adv.* **1,** e1501057, doi: 10.1126/sciadv.1501057.

Zhang, M., and L. Wen (2015). An effective method for small event detection: match and locate (M&L), *Geophys. J. Int.* **200,** 1523–1537.

Zhu, L., E. Liu, and J. H. McClellan (2017). A multi-channel approach for automatic microseismic event localization using RANSAC-based arrival time event clustering (RATEC), available at http://arxiv.org/abs/1702.01856 (last accessed June 2019).

Zhu, L., Z. Peng, J. McClellan, C. Li, D. Yao, Z. Li, and L. Fang (2019). Deep learning for seismic phase detection and picking in the aftershock zone of 2008 Mw 7. 9 Wenchuan earthquake, *Phys. Earth Planet. In.* doi: 10.1016/j.pepi.2019.05.004

Zhu, W., and G. C. Beroza (2019). PhaseNet: A deep-neural-network-based seismic arrival-time picking method, *Geophys. J. Int.* **216,** 261–273.

Miao Zhang[1]
William L. Ellsworth
Gregory C. Beroza
Department of Geophysics
Stanford University
397 Panama Mall
Stanford, California 94305 U.S.A.
mzhang18@stanford.edu
wellsworth@stanford.edu
beroza@stanford.edu

Published Online 11 September 2019

[1] Now at Department of Earth Sciences, Dalhousie University, 1355 Oxford Street, Halifax, Nova Scotia B3H 4J1, Canada; miao.zhang@dal.ca.